

Anomalous Nernst and Righi-Leduc effects in Mn_3Sn : Berry curvature and entropy flow

Xiaokang Li¹, Liangcai Xu¹, Linchao Ding¹, Jinhua Wang¹, Mingsong Shen¹, Xiufang Lu¹, Zengwei Zhu^{1,*} and Kamran Behnia^{1,2,*}

(1) Wuhan National High Magnetic Field Center

School of Physics, Huazhong University of Science and Technology,
Wuhan 430074, China

(2) Laboratoire de Physique Et d'Etude des Matériaux (UPMC-CNRS),
ESPCI Paris, PSL Research University
75005 Paris, France

(Dated: February 14, 2017)

We present a study of thermal and thermoelectric response in noncollinear antiferromagnet Mn_3Sn , which hosts a large Anomalous Hall Effect (AHE). Berry curvature generates zero-field off-diagonal thermal(Righi-Leduc) and thermoelectric(Nernst) signals, easily detectable at room temperature and invertible with a small magnetic field. The magnitude of the two Hall conductivities, thermal and electrical correlate according to the Wiedemann-Franz law. This implies that transverse currents generated by Berry curvature are carried by Fermi surface quasi-particles, as Haldane contended back in 2004. In contrast to Ni, the anomalous Lorenz number remains close to the Sommerfeld number over the whole temperature range of study, excluding any contribution by inelastic scattering as expected if Berry curvature were the unique source of AHE. The magnitude of the anomalous transverse thermoelectric response and its temperature dependence indicate that the locus of the asymmetrical Berry curvature shifts towards the Fermi level with cooling.

The ordinary Hall effect, the transverse electric field generated by a longitudinal charge current in presence of a magnetic field, is caused by the Lorentz force exerted by magnetic field on charge carriers. In ferromagnetic solids, there is an additional component to this response (known as extraordinary or anomalous), thought to arise as a result of a sizeable magnetization. During the past decade, a clear link between the Anomalous Hall Effect (AHE) and the Berry curvature of Bloch waves has been established[1, 2]. Recently, Chen, Niu and Macdonald[3] argued that in noncollinear antiferromagnets, one can find a large AHE without sizeable bulk magnetization. Experiments by Nakasutji *et al.*[4] and Nayak *et al.* [5] found that there is indeed a large AHE in Mn_3Sn [4] and Mn_3Ge [5, 6], which are noncollinear antiferromagnets at room temperature. Several recent theoretical studies were devoted to this issue and quantified the k-dependence of the Berry curvature from first-principle band theory[7–9].

In presence of magnetic field, a thermal gradient generates off-diagonal transport response too. Thermal conductance becomes a tensor with a transverse component, κ_{ij} , called the Righi-Leduc (or the thermal Hall) effect[10]. Thermoelectric conductance acquires also an off-diagonal component, α_{ij} , intimately linked to the Nernst coefficient, which is directly measurable by experiment[11]. These transverse coefficients are generated by the Lorentz force suffered by charged carriers of entropy. What happens to these off-diagonal coefficients when the Berry curvature replaces the magnetic field? Do they depend on the mean-free-path and on the thermal fuzziness of the Fermi surface?

In this letter, present a study of Anomalous Righi-Leduc (ARLE) and Nernst effects (ANE) in Mn_3Sn addressing these questions by quantifying the amplitude of these coefficients compared to their Hall counterpart. We detect a large Anomalous Righi-Leduc conductivity and find that its magnitude correspond to what is expected according to the Wiedemann-Franz Law over an extended temperature window. The result confirms a theoretical prediction by Haldane[12] with important consequences for the debate regarding the two alternative formulations of anomalous Hall effect[12–14]. AHE can be formulated as a property of the whole Fermi sea or the Fermi surface[12, 14]. The expected magnitude of the Anomalous Hall Conductivity (AHC) in both pictures is identical(at least in the case of BCC iron[15–17]). The verification of the Wiedemann-Franz law allows for an experimental distinction, since the validity of this law is straightforward in the Fermi-surface picture, but not necessarily in the Fermi-sea picture. Comparing our data to the results of a previous study of ARLE in Ni and $Ni_{0.97}Cu_{0.03}$ [18], we resolve a clear difference pointing to the absence of and inelastic scattering in generating the anomalous transverse response in Mn_3Sn . We also quantified the anomalous transverse thermoelectric response, α_{ij}^A , a quantity studied experimentally[19, 20] and theoretically[21] in ferromagnets. We argue that the magnitude and the temperature dependence of the ratio of σ_{ij}^{AH} to α_{ij}^{AN} imply that Weyl nodes, the sources and sinks of Berry curvature, are close to the Fermi level and become closer upon cooling.

The temperature dependence of the longitudinal transport properties of Mn_3Sn are shown in Fig. 1. As seen

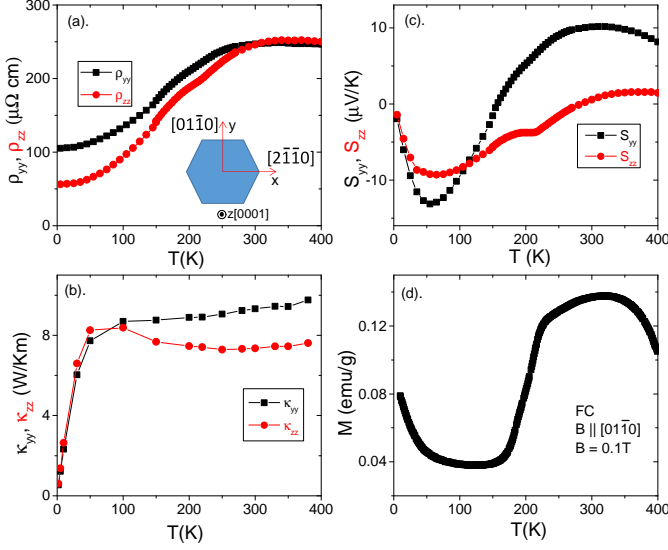


FIG. 1. (Color online) Temperature dependence of resistivity (a), thermal conductivity (b), Seebeck coefficient (c) and magnetization (d).

in the figure, resistivity attains a magnitude of $250 \mu\Omega$ cm and becomes almost flat at room temperature. Both electric and thermal conduction are almost isotropic, in contrast to the Seebeck coefficient. The temperature dependence of magnetization is similar to what was previously reported[22]. It shows that the system becomes magnetically ordered below $T_N=420$ K and above $T_1=200$ K with a weak ferromagnetic remanence. In 1980s, Tomiyoshi[23] studied the system by polarized neutron diffraction and found a triangular spin structure as originally suggested by Zimmer and Krén[24] and stabilized by the Dzyaloshinski-Moriya interaction.

Two points are to be noticed about transport of charge and entropy in this metal. First, given the carrier density ($n=2 \times 10^{22} \text{cm}^{-3}$ [4, 25]), a room-temperature resistivity of $250 \mu\Omega \text{cm}$ implies a mean-free-path as short as 0.7 nm. This is comparable to the lattice parameters ($a=0.566 \text{nm}$ and $c=0.453 \text{nm}$ [23]). Thus, the system is close to the Mott-Ioffe-Regel limit and the saturation of resistivity between 300 K and 400 K is not surprising[26]. Second, the room-temperature Lorenz number ($L_{ii} = \frac{\kappa_{ii}(300\text{K})\rho_{ii}(300\text{K})}{300}$) is almost twice the Sommerfeld number, $L_0 = 2.44 \times 10^{-8} \text{V}^2 \text{K}^{-2}$. Therefore, the total contribution of phonons and magnons to the longitudinal thermal transport is comparable to the electronic heat transport.

What makes this magnetic metal remarkable is its transverse transport, illustrated in Fig.2. With a current along [0001] (dubbed z-axis and) a magnetic field along [011̄0] (dubbed y-axis), there is a large and hysteretic jump in the Hall resistivity, ρ_{xz} . Its magnitude (7.6

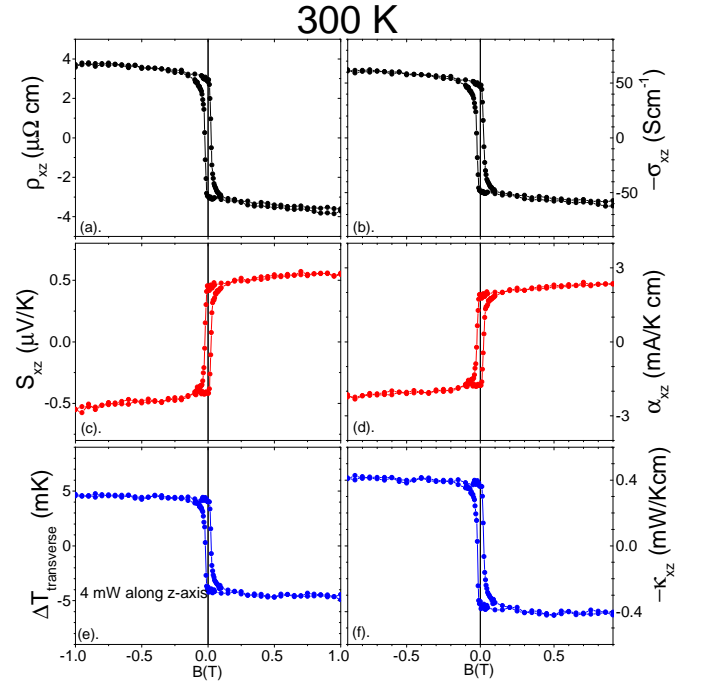


FIG. 2. (Color online) Room-temperature field dependence of transport coefficients. Magnetic field is applied along the y-axis ([011̄0]) and the charge (or heat) current along the z-axis ([0001]). a) Hall resistivity, ρ_{xz} , measured by measuring voltage along x-axis ([21̄1̄0]); b) Hall conductivity, σ_{xz} , extracted from ρ_{xz} , ρ_{xx} and ρ_{zz} ; c) Nernst signal, S_{xz} , the electric field along the x-axis divided by the thermal gradient along the z-axis; d) Transverse thermoelectric conductivity, α_{xz} , extracted from S_{xz} , S_{zz} , ρ_{xx} , ρ_{zz} and ρ_{xz} ; e) The transverse thermal gradient generated by a longitudinal heat current along the z-axis. f) The extracted Righi-Leduc coefficient, κ_{xz} .

$\mu\Omega \text{cm}$) is comparable to what was reported previously[4] and is reversible with a field as small as 0.1 T. The Nernst coefficient (Fig. 2c) shows a jump of $1 \mu\text{V/K}$, a remarkably large value, given the low mobility ($\sim 1.7 \text{cm}^2 \text{V}^{-1} \text{s}^{-1}$) and the large Fermi energy ($\sim 2.6 \text{eV}$) of the system, which yield a quasi-particle response six orders of magnitude lower[11]. The same set-up was used to measure the AHE and ANE in an iron single crystal at room temperature and data similar to what was previously reported[27, 28] was obtained. They are presented in Fig. S1 of the supplement[25]. Note how in Mn_3Sn , the anomalous transport coefficients dominate their ordinary counterparts, leading to a step-like profile quite distinct from what is seen in ferromagnets such as iron[27, 28] or cobalt[29].

From Hall resistivity, ρ_{xz} and Nernst response, S_{xz} , one can extract the magnitude of Hall conductivity, σ_{xz} (Fig. 2b), and transverse thermoelectric conductivity, α_{xz} (Fig. 2d). This can be done by manipulating $\bar{\rho}$, $\bar{\sigma}$, $\bar{\alpha}$ and \bar{S} tensors (See the supplement[25]). We also found a purely thermal counterpart to anomalous electric and

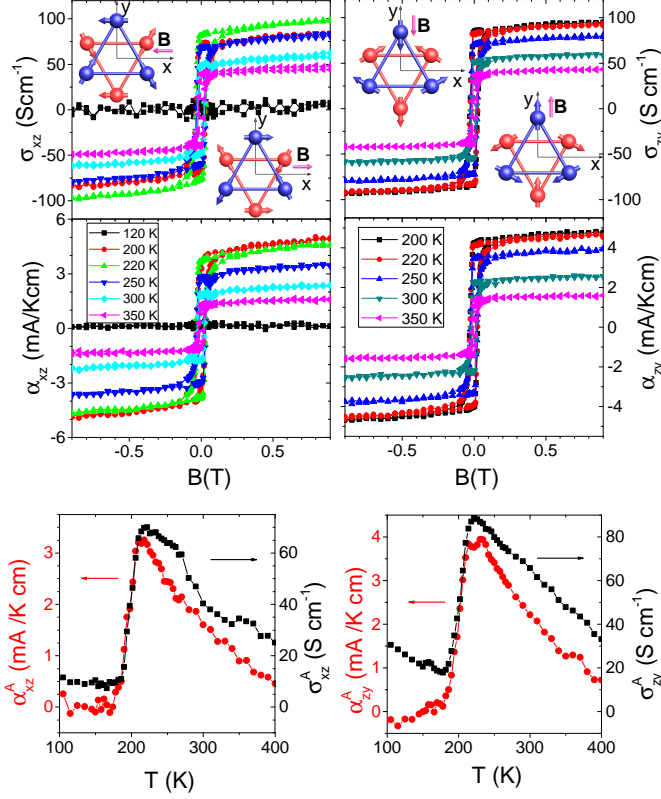


FIG. 3. (Color online) Top: Field dependence of σ_{xz} and α_{xz} (left) and σ_{zy} and α_{zy} (right) at different temperatures. The spin magnetic structure is sketched in the inset. Bottom: The temperature dependence of σ_{xz}^A and α_{xz}^A (left) and σ_{zy}^A and α_{zy}^A (right). Note the phase transition at $T^* \sim 200$ K leading to the collapse of all anomalous transport coefficients. For both orientations, α_{ij}^A raises faster than σ_{ij}^A .

thermoelectric responses. As seen in Fig.2e, applying a thermal current along the z-axis generates a transverse thermal gradient along the x-axis, which can be reverted by a magnetic field applied along the y-axis. This allows to extract the amplitude of thermal Hall (Righi-Leduc) conductivity, κ_{xz} (Fig. 2f).

The anomalous electric and thermoelectric transport coefficients were studied at different temperatures in two configurations (B//y and B//x). Fig. 3 presents the field dependence of σ_{xz} , σ_{zy} , α_{xz} and α_{zy} at several temperatures. As seen in the figure, the behavior remains step-like down to 200K and the magnitude of all coefficients smoothly increases with decreasing temperature. At $T_1 \simeq 200$ K, the triangular spin order is destroyed[30–32] and all anomalous transport coefficients disappear below this temperature as seen in the bottom panels of Fig. 3, which present the temperature dependence of σ_{ij}^A and α_{ij}^A . This confirms that the remarkably large magnitude of zero-field transverse transport coefficients is a property of the non-collinear antiferromagnet stabilised between

420 K and 200K. This phase transition to what seems to be a glassy ferromagnetic order[32, 33] at 200 K is specific to Mn_3Sn and does not occur in its sibling Mn_3Ge [5, 6]. In the following, we will focus on the magnitude of the anomalous transport coefficients in the magnetic phase hosting the triangular spin order. Two correlations are relevant here. The first is the Wiedemann-Franz law:

$$\kappa_{ij}^A/T\sigma_{ij}^A = L_0 = \frac{\pi^2}{3} \left(\frac{k_B}{e}\right)^2 \quad (1)$$

The second is the Mott formula:

$$\alpha_{ij} = -\frac{\pi^2}{3} \frac{k_B}{e} k_B T \frac{\partial \sigma_{ij}}{\partial E} \Big|_{E_F} \quad (2)$$

Fig. 4 presents the field dependence of κ_{xz} and κ_{zy} at different temperatures and the temperature dependence of anomalous Lorenz number, $L_{ij}^A = \kappa_{ij}^A/T\sigma_{ij}^A$. As one can see in the bottom panels of Fig. 4, the magnitude of experimentally resolved L_{ij}^A remains close to L_0 between 200K and 400K, where we see the anomalous transverse response. Thus, the two Anomalous Hall conductivities, thermal and electrical obey the correlation dictated by the Wiedemann-Franz law. As mentioned above, the ordinary longitudinal coefficients do not present such a correlation, as a result of sizeable contribution to heat transport by phonons and/or magnons. Let us consider the consequences of a finite anomalous Righi-Leduc effect. The intrinsic AHE arises as result of an additional term in the group velocity of Bloch electrons[36]:

$$\dot{r} = \frac{1}{\hbar} \frac{\partial \epsilon_n(\mathbf{k})}{\partial \mathbf{k}} + \dot{\mathbf{k}} \times \Omega_n(\mathbf{k}) \quad (3)$$

Here, $\Omega_n(\mathbf{k})$ is the local Berry curvature. In presence of an electric field, E , $\dot{\mathbf{k}} = -eE/\hbar$. Starting from this, one can derive the an expression for σ_{ij}^A in presence of Berry curvature, Ω_n^k (n is a band index)[1, 2, 21]:

$$\sigma_{ij}^A = \frac{-e^2}{\hbar} \sum_n \int_{BZ} \frac{d^3k}{(2\pi)^3} f_n(k) \Omega_n^k(k) \quad (4)$$

The expression is similar to the topological formulation of the Quantum Hall effect[37]. Note that the integral is taken over the whole Brillouin zone (BZ). Haldane[12] noticed that according to such an expression, AHE is a property of the whole Fermi sea and not the Fermi surface, as one would expect in the spirit of Landau's Fermi liquid theory. He proposed the following expression [12, 14]:

$$\sigma_{ij}^A = \frac{-e^2}{\hbar} \sum_n \int_{S_n} \frac{d^2k}{(2\pi)^2} [\Omega_n^k(k) \cdot \hat{n}(k)] \mathbf{k} \quad (5)$$

Here, the integral is taken over the Fermi surface S_n of band n and $\hat{n}(k)$ is the unit vector perpendicular to

the surface. The two formulations of σ_{xy}^A yield quasi-identical values in the case of BCC-iron[15], both close to the experimental value[25, 27]. A temperature gradient can act like an electric field and generate a force, if the electronic states in question possess an entropy, S_k leading to $\dot{\mathbf{k}} = -S_k \nabla T / \hbar$ and a finite κ_{ij}^A . Now, in a Fermi-Dirac distribution the interface between occupied and unoccupied states is the only reservoir of entropy[35]. In other words, only states at the Fermi surface (and not those deep inside the Fermi sea) can feel a force exerted by a temperature gradient. The validity of the Wiedemann-Franz law implies that the transverse electronic flow generated by Berry curvature is a flow of charge and entropy with a ratio of $\frac{\pi^2}{3} \left(\frac{k_B}{e}\right)^2$. This rules out any contribution to σ_{ij}^A by Weyl nodes of the entirely occupied bands, the central issue in the Fermi-sea vs. Fermi-surface debate[13, 14].

Previous to this study, Onose *et al.*[18] measured the anomalous thermal Hall conductivity of ferromagnetic Ni and Ni_{0.97}Cu_{0.03} and found that the Wiedemann-Franz law is satisfied at low temperatures. Their data is compared to ours in the lower panels of Fig.4. As one can see in the figure, in those systems, L_{ij}^A is close to L_0 in the zero-temperature limit and shows a steady downward trend at finite temperature. Now, Wiedemann-Franz law is only valid in absence of inelastic scattering[38]. The Lorenz-Sommerfeld ratio is expected to deviate downward from unity in presence of inelastic scattering. As one can see in Fig.4, such a deviation is clearly present in the Ni and Ni_{0.97}Cu_{0.03}[18] data but not in Mn₃Sn. This implies that inelastic scattering plays a role in generating the room-temperature anomalous transverse response in those two ferromagnets, but not in Mn₃Sn. Now, there are two known mechanisms for AHE, one expressed in terms of the Berry-phase curvature is an intrinsic property of a perfect crystal. The second is an extrinsic mechanism, invoking skew scattering[1]. Only in the first case (i.e. when AHE is solely generated by Berry curvature), no inelastic scattering is expected. Skew scattering by magnons for example is an extrinsic process, which may play a partial role in the case of Ni and Ni_{0.97}Cu_{0.03} but not in Mn₃Sn. Thus the observation of a temperature-independent L_{ij}^A/L_0 in Mn₃Sn not only excludes a phonon contribution[34], but also, and in contrast to conventional ferromagnets, any contribution due to inelastic skew scattering.

Let us now consider the magnitude of α_{ij}^A . According to the Mott formula, α_{ij}^A is proportional to the energy derivative of σ_{ij}^A [11, 20, 21, 35], a quantity inaccessible to a DC transport experiment. It provides insight regarding the temperature dependence of the two transverse coefficients. Low-field ordinary Hall conductivity is proportional to the square of the mean-free-path[11, 39]. On the other hand, topological Hall conductivity, as in the case of Quantum Hall effect [37], does not depend

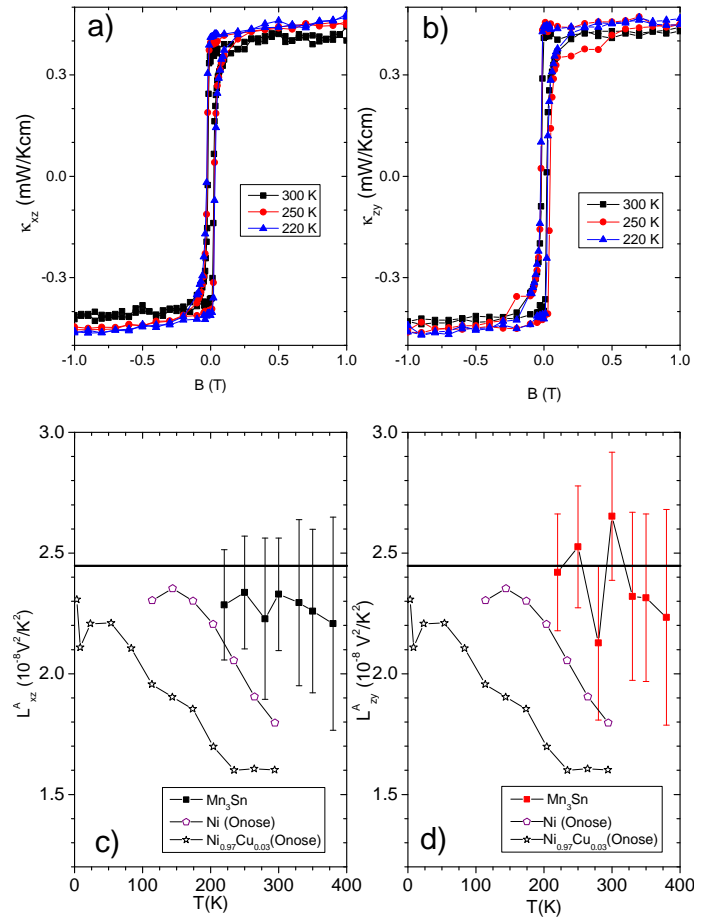


FIG. 4. (Color online)- Top: The field-dependence of κ_{yz} (a) and κ_{zx} (b) at different temperatures (more data at other temperatures are in the supplement[25]). Bottom: The temperature dependence of anomalous Lorenz number L_{zx}^A (c) and L_{yz}^A (d). Also shown are the anomalous Lorenz number of Ni and Ni_{0.97}Cu_{0.03} according to ref.[18].

on the mean-free-path. If the AHE measured here is a topological property of the electronic system and independent of the carrier-mean-free-path, why does its magnitude increase with cooling? A similar question can be asked about the temperature dependence of ANE. Ordinary Nernst response roughly scales with $k_B T / E_F$ [11]. Why does α_{ij}^A increase with cooling? And why does it so faster than σ_{ij}^A (See Fig. 3)? The ratio $\alpha_{ij}^A / \sigma_{ij}^A$ evolves from $15 \mu V / K$ at room temperature to $50 \mu V / K$ around 220K, a sizeable fraction of $k_B / e = 86 \mu V / K$ and much larger than $k_B T / E_F$. Magnetization is flat in the same temperature window. But, the Weyl nodes may shift as a result of thermal contraction. This may be the source of the temperature dependence of σ_{ij}^A and its energy derivative. Checking this hypothesis is a challenge for first-principle theories of Mn₃Sn[7–9].

In summary, we have detected thermal and thermoelec-

tric transverse responses generated by Berry curvature in Mn_3Sn and found that the Wiedemann-Franz law is valid with no sign of downward finite-temperature deviation, expected and observed in presence of inelastic scattering. This implies that not only the electrical Hall current has a purely thermal counterpart carried by Fermi surface quasi-particles, but also that it has a purely intrinsic origin in contrast to Ni and $\text{Ni}_{0.97}\text{Cu}_{0.03}$.

We acknowledge useful discussions with M. O. Goerbig. Z. Z. was supported by the 1000 Youth Talents Plan and the work was supported by the National Science Foundation of China (Grant No. 11574097) and The National Key Research and Development Program of China (Grant No. 2016YFA0401704). K. B was supported by China High-end foreign expert programme and Fonds-ESPCI-Paris.

* zengwei.zhu@hust.edu.cn

* kamran.behnia@espci.fr

-
- [1] N. Nagaosa, J. Sinova, S. Onoda, A. H. MacDonald and N. P. Ong, *Rev. Mod. Phys.* **82**, 1539 (2010).
- [2] D. Xiao, M.-C. Chang, and Q. Niu, *Rev. Mod. Phys.* **82**, 1959 (2010).
- [3] H. Chen, Q. Niu, and A. MacDonald, *Phys. Rev. Lett.* **112**, 017205 (2014).
- [4] S. Nakatsuji, N. Kiyohara, and T. Higo, *Nature* **527**, 212 (2015).
- [5] A. K. Nayak *et al.*, *Sci. Adv.* **2**: e1501870 (2016).
- [6] N. Kiyohara, T. Tomita, and S. Nakatsuji, *Phys. Rev. Appl.* **5**, 064009 (2016).
- [7] J. Kübler and C. Felser, *Europhys. Lett.* **108**, 67001 (2014).
- [8] Y. Zhang *et al.*, arXiv:1610.04034 (2016).
- [9] M.-T. Suzuki, T. Koretsune, M. Ochi and R. Arita, arXiv:1611.06042 (2016).
- [10] Y. Zhang, N. P. Ong, Z. A. Xu, K. Krishana, R. Gagnon and L. Taillefer, *Phys. Rev. Lett.* **84**, 2219 (2000)
- [11] K. Behnia and H. Aubin, *Rep. Prog. Phys.* **79**, 046502 (2016).
- [12] F. D. M. Haldane, *Phys. Rev. Lett.* **93**, 206602 (2004).
- [13] Y. Chen, D. L. Bergman, and A. A. Burkov, *Phys. Rev. B* **88**, 125110 (2013).
- [14] D. Vanderbilt, I. Souza, and F. D. M. Haldane, *Phys. Rev. B* **89**, 117101 (2014).
- [15] D. Gosálbez-Martínez, I. Souza, and D. Vanderbilt, *Phys. Rev. B* **92**, 085138 (2015).
- [16] Y. Yao *et al.*, *Phys. Rev. Lett.* **92**, 037204 (2004).
- [17] X. Wang, J. R. Yates, I. Souza, and D. Vanderbilt, *Phys. Rev. B* **74**, 195118 (2006).
- [18] Y. Onose, Y. Shiomi, and Y. Tokura, *Phys. Rev. Lett.* **100**, 016601 (2008)
- [19] W.-L. Lee, S. Watauchi, V. L. Miller, R. J. Cava, and N. P. Ong, *Phys. Rev. Lett.* **93**, 226601 (2004).
- [20] T. Miyasato *et al.*, *Phys. Rev. Lett.* **99**, 086602 (2007).
- [21] D. Xiao, Y. Yao, Z. Fang, and Q. Niu, *Phys. Rev. Lett.* **97**, 026603 (2006).
- [22] H. Ohmori, S. Tomiyoshi, H. Yamauchi and H. Yamamoto, *J. Magnet. Magnet. Mat.* **70**, 249 (1987).
- [23] S. Tomiyoshi, *J. Phys. Soc. Jpn.* **51**, 803 (1982); S. Tomiyoshi, and Y. Yamaguchi, *J. Phys. Soc. Jpn.* **51**, 2478 (1982).
- [24] G. J. Zimmer and E. Krén, *AIP Conf. Proceed.* **10**, 1379 (1973).
- [25] See the supplemental material.
- [26] O. Gunnarsson, M. Calandra and J. E. Han, *Rev. Mod. Phys.* **75**, 1085 (2003).
- [27] P. N. Dheer, *Phys. Rev.* **156**, 637 (1967).
- [28] S. J. Watzman *et al.*, *Phys. Rev. B* **94**, 144407 (2016).
- [29] J. Kötzler and W. Gil, *Phys. Rev. B* **72**, 060412(R) (2005).
- [30] E. Krén, J. Paitz, G. Zimmer, and É. Zsoldos, *Physica B+C* **80**, 226 (1975).
- [31] S. Tomiyoshi, S. Abe, Y. Yamaguchi, H. Yamauchi, and H. Yamamoto, *J. Magnet. Magnet. Mat.* **54**, 1001 (1986).
- [32] P. J. Brown, V. Nunez, F. Tasset, J. B. Forsyth, and P. Radhakrishna, *J. Phys.: Condens. Matt.* **2**, 9409 (1990).
- [33] W. J. Feng *et al.*, *Phys. Rev. B* **73**, 205105 (2006)
- [34] C. Strohm, G. L. J. A. Rikken, and P. Wyder, *Phys. Rev. Lett.* **95**, 155901(2005).
- [35] K. Behnia, *Fundamentals of thermoelectricity*, Oxford University Press (2015).
- [36] M.-C. Chang and Q. Niu, *Phys. Rev. B* **53**, 7010 (1996)
- [37] M. Kohmoto, *Ann. Phys.* **160**, 343 (1985).
- [38] J. Ziman, *Principles of the Theory of Solids*, Cambridge University Press (1972).
- [39] N. P. Ong, *Phys. Rev. B* **43**, 193 (1991).

Samples and experimental methods

The Mn_3Sn single crystal was grown using the Bridgman-Stockbarger technique. The raw materials, Mn (99.99% purity) and Sn (99.999%), were weighed and mixed inside an Ar glove box with a molar ratio of 3.1:1. After being sealed in a quartz ampule, they were loaded into an alumina crucible. The growth temperature was controlled at the bottom of the ampule. The material was heated up to 1100 °C. remained there for 2 hour to ensure homogeneity of the melt, and was cooled slowly to 950 °C. It was annealed at that temperature for 40 hours afterwards. Finally, it was gently cooled down back to room temperature. The single crystals were cut by a wire saw into $0.5 \times 0.5 \times 2\text{mm}^3$ dimensions for transport measurements. The iron single crystal with 99.99% purity was obtained commercially. The thermal conductivity measurements were done with a one-heater-two-thermometers technique in PPMS with a high-vacuum environment. Two Chromel-constantan (type E) thermocouples were employed to measure the temperature difference generated by a small heater chip. We measured the other transport coefficients separately from thermal conductivity measurement. The voltage was monitored by DC-nanometers and electric current was driven by a current source. Generally, the temperature gradient is around 5 K/cm. The procedure of zero-field transport coefficients were obtained as the

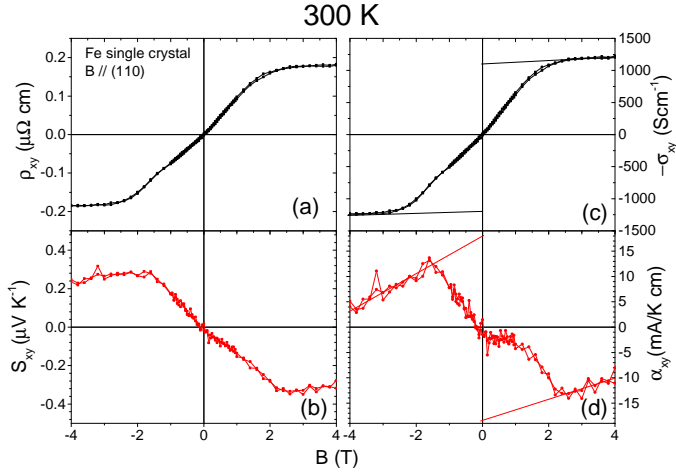


FIG. 5. Anomalous Hall effect and Anomalous Nernst effect (bottom) in BCC Iron at room temperature. By extrapolating the slope of the high-field response, one can extract $\sigma_{xz}^A(300K)$ and $\alpha_{xy}^A(300K)$.

reported[4] by cooling down the temperature to 5K with a field 7T(-7T), decreasing to +0T(-0T), then starting to measure at different temperatures. The coefficients were finally gotten by being symmetrized(antisymmetrized) accordingly from the raw data. The magnetization measurement was also carried out in PPMS with VSM option with 0.1T field-cooling.

Carrier density and mean-free-path

The normal Hall conductivity, extracted from the slope of $\sigma_{xz}(B)$ allows to estimate the Hall coefficient, R_H . This leads to a carrier density of $n=2 \times 10^{22} \text{cm}^{-3}$, close to what was reported previously[4]. With this carrier density, and $\rho(300K) = 250 \mu\Omega \text{cm}$, one finds a room-temperature mean-free-path of 0.7 nm.

ANE and AHE in iron

Room-temperature field dependence of Hall resistivity and Nernst coefficient in an iron crystal is presented in Fig.S1. The results are similar to an early study of AHE[27] and a very recent study of ANE[28] in iron. We find $\sigma_{xz}^A(300K) = 1200 \text{S/cm}$, compared to 1200 S/cm reported by Dheer[27] and 755 S/cm according to several theoretical calculations[15–17]. The magnitude of $\alpha_{xy}^A(300K)$ was found to be 18 mA/K cm.

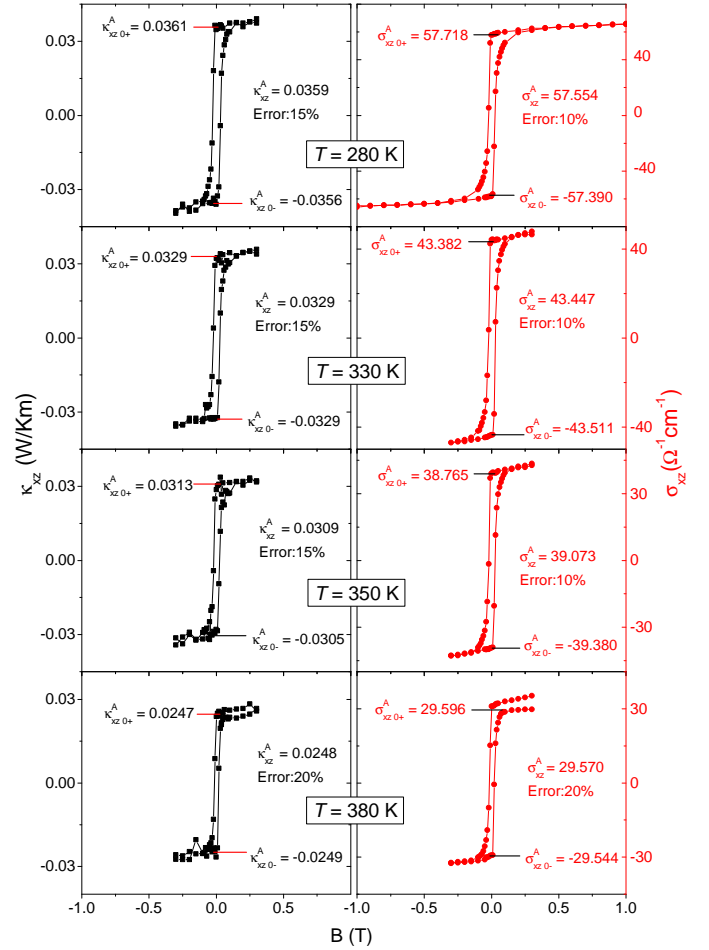


FIG. 6. The field-dependence of κ_{xz} and σ_{xz} at different temperature.

More raw data at different temperatures for field-dependence of the transverse thermal and electric conductivity

The raw data at different temperatures is presented here. Fig. S2 shows the field dependence of κ_{xz} and σ_{xz} , while the Fig. S3 shows the field dependence of κ_{zy} and σ_{zy} . The large error margin at 380K is due to a long waiting time and unavoidable temperature drift.

Deriving off-diagonal components of $\bar{\sigma}$, $\bar{\alpha}$ and $\bar{\kappa}$

The off-diagonal component of the Peltier-Ettingshausen tensor, $\bar{\alpha}$, is linked to the charge current density, \vec{J}_e , the electric field, \vec{E} , the thermal gradient, $\vec{\nabla}T$ and the electric conductivity tensor, $\bar{\sigma}$, through:

$$\vec{J}_e = \bar{\sigma} \vec{E} - \vec{\nabla}T \bar{\alpha} \quad (6)$$

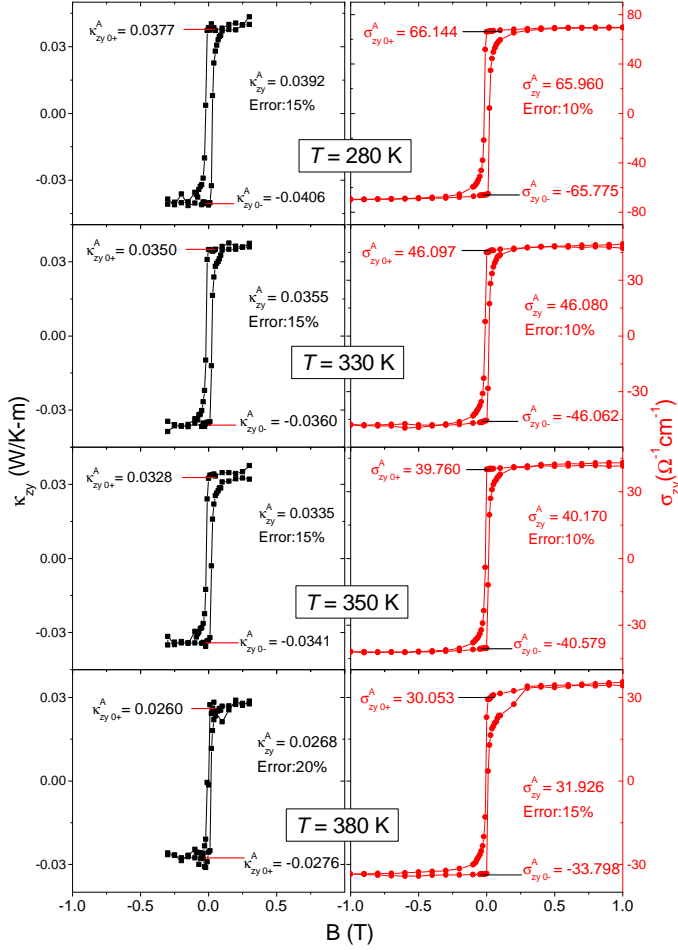


FIG. 7. The field-dependence of κ_{zy} and σ_{zy} at different temperature.

In absence of temperature gradient, $\nabla T = 0$, the tensor $\bar{\sigma}$ can be obtained from measurable resistivity tensor $\bar{\rho}$:

$$\bar{\sigma} = \bar{\rho}^{-1}. \quad (7)$$

In absence of charge current density, one finds that the Seebeck-Nernst tensor \bar{S} is linked to $\bar{\alpha}$ and $\bar{\sigma}$ in the following manner:

$$\bar{S} = \bar{\sigma}^{-1} \bar{\alpha} = \bar{\rho} \bar{\alpha} \quad (8)$$

Therefore, combining the measured components of \bar{S} with those of the resistivity tensor, $\bar{\rho}$, one can compute the components of $\bar{\alpha}$. Specifically, for sample 1: when the magnetic field along y axis([01 $\bar{1}$ 0] in the our case), the electric and thermal current along z axis[0001] and the transverse voltage along x axis[2 $\bar{1}$ 10].

When the electric field is applied along z axis:

$$\begin{aligned} \bar{\sigma} &= \bar{\rho}^{-1} = \begin{pmatrix} \rho_{xx} & \rho_{xz} \\ \rho_{zx} & \rho_{zz} \end{pmatrix}^{-1} \\ &= \frac{1}{\rho_{xx}\rho_{zz} - \rho_{xz}\rho_{zx}} \begin{pmatrix} \rho_{zz} & -\rho_{xz} \\ -\rho_{zx} & \rho_{xx} \end{pmatrix} = \begin{pmatrix} \sigma_{xx} & \sigma_{xz} \\ \sigma_{zx} & \sigma_{zz} \end{pmatrix} \end{aligned}$$

The Hall conductivity can be deduced as the following:

$$\sigma_{xz} = \frac{-\rho_{xz}}{\rho_{xx}\rho_{zz} - \rho_{xz}\rho_{zx}}.$$

Since $\rho_{xz} = -\rho_{zx}$, and ρ_{xz}^2 is negligibly small comparing to the longitude resistivity in the current case.

$$\sigma_{xz} \approx \frac{-\rho_{xz}}{\rho_{xx}\rho_{zz}}. \quad (9)$$

When there is a temperature gradient, but no electric current along the z-axis:

$$\begin{aligned} \bar{\alpha} &= \bar{\rho}^{-1} \bar{S} = \begin{pmatrix} \rho_{xx} & \rho_{xz} \\ \rho_{zx} & \rho_{zz} \end{pmatrix}^{-1} \begin{pmatrix} S_{xx} & S_{xz} \\ S_{zx} & S_{zz} \end{pmatrix} \\ &= \frac{1}{\rho_{xx}\rho_{zz} - \rho_{xz}\rho_{zx}} \begin{pmatrix} \rho_{zz} & -\rho_{xz} \\ -\rho_{zx} & \rho_{xx} \end{pmatrix} \begin{pmatrix} S_{xx} & S_{xz} \\ S_{zx} & S_{zz} \end{pmatrix} \\ &= \frac{1}{\rho_{xx}\rho_{zz} - \rho_{xz}\rho_{zx}} \begin{pmatrix} \rho_{zz}S_{xx} - \rho_{xz}S_{zx} & \rho_{zz}S_{xz} - \rho_{xz}S_{zz} \\ -\rho_{zx}S_{xx} + \rho_{xx}S_{zx} & -\rho_{zx}S_{xz} + \rho_{xx}S_{zz} \end{pmatrix} \\ &= \begin{pmatrix} \alpha_{xx} & \alpha_{xz} \\ \alpha_{zx} & \alpha_{zz} \end{pmatrix} \end{aligned}$$

So the off-diagonal term can be written as following:

$$\alpha_{xz} = \frac{\rho_{zz}S_{xz} - \rho_{xz}S_{zz}}{\rho_{xx}\rho_{zz} - \rho_{xz}\rho_{zx}} \approx \frac{\rho_{zz}S_{xz} - \rho_{xz}S_{zz}}{\rho_{xx}\rho_{zz}}. \quad (10)$$

Using the measured known components of the resistivity and the Seebeck-Nernst tensor, α_{xz} can be obtained.

To obtain the thermal Hall coefficient, the thermal current can be written as following when only temperature gradient is present:

$$\vec{J}_q = -\bar{\kappa} \nabla T$$

$$\begin{pmatrix} J_{qx} \\ J_{qz} \end{pmatrix} = - \begin{pmatrix} \kappa_{xx} & \kappa_{xz} \\ \kappa_{zx} & \kappa_{zz} \end{pmatrix} \begin{pmatrix} \partial_x T \\ \partial_z T \end{pmatrix}$$

Because thermal current density along z axis, we obtain:

$$0 = -\kappa_{xx}\partial_x T - \kappa_{xz}\partial_z T$$

$$J_{qz} = -\kappa_{zx}\partial_x T - \kappa_{zz}\partial_z T$$

So the thermal current density can be obtained:

$$J_{qz} = \frac{\nabla_x T}{\kappa_{xz}} (\kappa_{xx}\kappa_{zz} + \kappa_{xz}^2)$$

Since $\kappa_{xz} \ll \kappa_{xx}$ or κ_{zz} , we can drop the κ_{xz}^2 term. With $J_{qz} = I^2 R / (wt)$, where t, w is the thickness, width of the sample respectively. The Righi-Leduc coefficient can be inferred:

$$\kappa_{xz} = \frac{\partial_x T \kappa_{xx} \kappa_{zz}}{J_{qz}} = -\frac{\kappa_{xx}(B) \kappa_{zz}(B) \Delta_x T(B) t}{I^2 R} \quad (11)$$

The same procedure can be used for a second configuration: the magnetic field is along x axis, the electric and thermal current along y axis and the transverse voltage along z axis. One would derive the following expressions

for σ_{zy} , α_{zy} and κ_{zy} :

$$\sigma_{zy} \approx \frac{-\rho_{zy}}{\rho_{yy} \rho_{zz}}. \quad (12)$$

$$\alpha_{zy} \approx \frac{\rho_{yy} S_{zy} - \rho_{zy} S_{yy}}{\rho_{yy} \rho_{zz}}. \quad (13)$$

$$\kappa_{zy} = -\frac{\kappa_{yy}(B) \kappa_{zz}(B) \Delta_z T(B) t_2}{I^2 R} \quad (14)$$